

Evaluating the Accuracy of Jason-3 Water Vapor Product Using PWV Data from Global Radiosonde and GNSS Stations

Yangzhao Gong^{1,2}, Zhizhao Liu^{1,2}

¹Department of Land Surveying & Geo-Informatics (LSGI), The Hong Kong Polytechnic University (PolyU), 181 Chatham Road South, Hung Hom, Kowloon, Hong Kong, P. R. China

²Research Institute for Sustainable Urban Development, The Hong Kong Polytechnic University (PolyU), 181 Chatham Road South, Hung Hom, Kowloon, Hong Kong, P. R. China

Corresponding author: Zhizhao Liu

Tel: (852)2766 5961 (Office) Fax: (852)2330 2994

E-mail: lszzliu@polyu.edu.hk

Key points of this study:

- 1, More than 3-year Jason-3 AMR water vapor products are evaluated at a global scale using 263 radiosonde stations and 103 GNSS stations.
- 2, The Jason-3 water vapor accuracies evaluated by radiosonde and GNSS are 3.4 and 3.0 kg/m², respectively.
- 3, The accuracy of Jason-3 water vapor data varies with season, latitude and its distance to land.

Abstract: Jason-3 is equipped with an Advanced Microwave Radiometer (AMR) to remove the signal wet delay caused by precipitable water vapor (PWV). In order to investigate the accuracy of PWV from Jason-3 AMR on a global scale, we adopt PWV observations from 263 radiosonde stations and 103 GNSS stations as reference PWV. These reference PWV are recorded during Jason-3 cycles 0 – 119 and are globally distributed in coastal and island regions. Over 60,000 Jason-3 PWV vs radiosonde PWV comparison points and over 380,000 Jason-3 PWV vs GNSS PWV comparison points are used in this study. For GNSS PWV, four retrieval strategies are used to retrieve GNSS PWV: a combination of two different zenith hydrostatic delay (ZHD) modeling methods (Saastamoinen and ECMWF), and two PWV height reduction methods (Kouba empirical method and ECMWF method to reduce PWV from height of station to sea level). The comparison results indicate that the root mean square error (RMSE) of Jason-3 PWV evaluated using radiosonde PWV is 3.4 kg/m², while the RMSE evaluated with PWV from four different GNSS schemes are in the range of 3.0 – 3.5 kg/m². Specifically, Jason-3 PWV has the best agreement (3.0 kg/m² of RMSE) with GNSS PWV derived using Saastamoinen ZHD correction and ECMWF PWV height correction. In addition, the accuracy of Jason-3 PWV increases when the latitude of its footprints or the distance from its footprints to land increases. The correlation coefficient of Jason-3 PWV with radiosonde and GNSS PWV are 0.984 and 0.988, respectively.

Keywords: Jason-3, Advanced Microwave Radiometer, Precipitable Water Vapor, GNSS, Radiosonde,

1 Introduction

As an essential component of atmosphere, precipitable water vapor (PWV) plays an important role in climate change (Zhang et al., 2013), protecting environment (Wang et al., 2016), radio-based geodetic technique (Wang & Liu, 2019), and many other areas. Currently, ground-based PWV observation systems, such as Global Navigation Satellite Systems (GNSS) networks, have provided a large volume of PWV data over continental lands with reasonably good global coverage. However, it is challenging to make PWV observation over the vast ocean regions. In the oceanographic and geodetic community, a number of satellite missions have been launched, such as the altimetry satellites (Lambin et al., 2010; Maiwald et al., 2016). These satellites normally are equipped with a microwave radiometer in order to correct the range delay caused by atmospheric water vapor. In addition to the correction of altimetry data, water vapor radiometers onboard altimetry satellites offer a valuable source of water vapor measurements over the vast ocean regions. These measurements, complementing the ground-based water vapor observations, make a significant contribution to the weather forecasting, climate studies and others.

GEOSAT (GEOdetic SATellite) is the first altimetry mission providing long-term altimetry observations. It was launched in March 1985 and ended its services in January 1990. After that, a series of altimetry missions were launched or are planned. These altimetry missions are summarized in Table 1. Among seven current altimetry missions, Jason-3 has relatively short repeat orbit (around 9.9 days). This means that Jason-3 can provide PWV observations with higher temporal resolution. In addition, the Jason-3 is equipped with a 3-band radiometer, while the radiometer in Sentinel-3A, Sentinel-3B, SARAL is working in 2-band (Fernandes et al., 2015). Another altimetry mission with 3-band radiometer is the HY-2A. No radiometer is embarked on Cryosat-2 or CFOSAT. In this study, Jason-3 is selected to be evaluated because of its superior performance in PWV monitoring.

Table 1 A list of past, current, future altimetry missions

	Altimetry mission	Launch date – Decommission date
Past missions	GEOSAT	1985-1990
	ERS-1 (European Remote Sensing Satellite-1)	1991-1996
	TOPEX/Poseidon	1992-2005
	GFO (Geosat Follow-On)	1998-2008
	ERS-2	1995-2011
	Envisat (Environmental Satellite)	2002-2012
	Jason-1	2001-2013

	SPOT (Including 5 satellites)	SPOT 1: 1986-2001, SPOT 2: 1990-2009 SPOT 3: 1993-1996, SPOT 4: 1998-present SPOT 5: 2002-present
	Ocean Surface Topography Mission (OSTM)/Jason-2	2008-2019
Current missions	Cryosat-2	2010-present
	HY-2A (Haiyang-2A)	2011-present
	SARAL (Satellite with ARgos and ALtika)	2013-present
	Jason-3	2016-present
	Sentinel-3A	2016-present
	Sentinel-3B	2018-present
	CFOSAT (Chinese-French Oceanic SATellite)	2018-present
Future missions	SWOT (Surface Water Ocean Topography)	Planned in 2021
	Jason-CS/Sentinel-6 (Including 2 satellites)	Jason-CS/Sentinel-6A: planned in 2020 Jason-CS/Sentinel-6B: planned in 2026

Jason-3 satellite was launched by a joint mission by the Centre National d'Études Spatiales (CNES), the United States National Aeronautics and Space Administration (NASA), the European Organisation for the Exploitation of Meteorological Satellites (EUMETSAT) and the National Oceanic and Atmospheric Administration (NOAA) on 17 January 2016. It is the follow-on mission to the TOPEX/Poseidon, Jason-1, and OSTM/Jason-2 and the 4th satellite in the TOPEX/Poseidon and Jason series. It takes an important responsibility of monitoring the change of sea level and collecting the oceanic meteorological observations. To monitor the change of sea level accurately, a 3-channel Advance Microwave Radiometer (AMR) operating at frequencies 18.7, 23.8, and 34.0 GHz is used to Jason-3 to correct the zenith wet delay (ZWD) caused by water vapor along the signal path (Maiwald et al., 2016). Compared with AMR onboard on OSTM/Jason-2, Jason-3 AMR is more stable and has better performance in instrument thermal control (Maiwald et al., 2016). The Jason-3 AMR is expected to have a better performance than its previous generation on TOPEX and Jason satellites, i.e., TOPEX/Poseidon Microwave Radiometer (TMR), Jason-1 Microwave Radiometer (JMR) as well as OSTM/Jason-2 AMR.

However, we find that investigation on the performance of Jason-3 AMR is very little. A study reported by (Fernandes & Lázaro, 2018) showed that Jason-3 ZWD has a root mean square error (RMSE) of 1.3 cm compared with Sentinel-3A ZWD. For the previous missions, a large number of comprehensive evaluations have been conducted to analyze the accuracy of ZWD from TOPEX/Poseidon TMR, Jason-1 JMR and OSTM/Jason-2 AMR (Brown et al., 2004; Chambers et al., 2003; Ruf et al., 1994;

Sibthorpe et al., 2011). Ruf et al. (1994) estimated that the RMSE of TOPEX/Poseidon TMR measured ZWD was at around 1.1 cm by making comparison with ZWD from ground-based microwave water vapor radiometers and radiosonde. Keihm et al. (2000) evaluated the performance of TOPEX/Poseidon TMR during 1992-1998 using the ZWD from 15 island radiosondes and the special sensor microwave imager (SSM/I) instruments. Based on the comparison results, they concluded that the offset between TMR ZWD and SSM/I ZWD or radiosonde ZWD is less than 10 mm. For Jason-1 JMR, evaluations have also been conducted in the past studies. In 2003, an experiment at Harvest, California, USA (34.47° N, -120.67° E) found that 1 cm-level agreement was found between both TMR ZWD and JMR ZWD and GNSS ZWD (Haines et al., 2003). Compared with Jason-1 JMR, OSTM/Jason-2 AMR has been proved to have a more stable performance than JMR (Ablain et al., 2010). Sibthorpe et al. (2011) compared ZWD from OSTM/Jason-2 AMR at 148 GNSS stations located at islands and coasts and a 6% of scale difference between OSTM/Jason-2 ZWD and GNSS ZWD was reported.

Previous studies have demonstrated that radiometers aboard on TOPEX/Jason series satellites are able to achieve a satisfying accuracy. However, the radiometer's performance degraded dramatically near the land because of significantly different emissivities for land (over 0.9) and for ocean (near 0.5) between 18 to 34 GHz (Brown, 2010). Given the accuracy degradation caused by land contamination, ZWD measurements of Jason-2 near coastal regions are flagged as invalid if that contamination leads to ZWD difference larger than 5 mm when compared to the backup ZWD from ECMWF (the European Centre for Medium range Weather Forecasts) (Brown, 2010; Sibthorpe et al., 2011). Normally, the ZWD values of TOPEX/Poseidon TMR and Jason-1 JMR are treated as invalid when the distance between their footprints and coastlines is shorter than 50 km, while the corresponding distance is around 25 km for OSTM/Jason-2 AMR (Brown, 2010; Brown et al., 2004). In order to improve the accuracy of OSTM/Jason-2 ZWD product near coastline, an improved ZWD retrieval algorithm was developed (Brown, 2010). Using this algorithm, the ZWD error can be smaller than 0.8 cm, 1.0 cm, 1.2 cm when the footprint of OSTM/Jason-2 AMR is 15 km, 10 km, 5 km far from land, respectively. At the coastline, the error can be smaller than 1.5 cm using this algorithm (Brown, 2010). Other attempts have also been made to improve the accuracy of altimetry satellite PWV in the coastal regions by using ground-based GNSS observations (Fernandes et al., 2010, 2015).

Recently, several studies utilized shipborne GNSS PWV to evaluate the accuracy of altimetry satellites, e.g. HY-2A, SARAL. Liu et al. (2019) reported a 0.8 kg/m² of agreement between PWV derived from shipborne GPS/GLONASS observations and HY-2A calibration microwave radiometer (CMR) during a two-month cruise in the Indian Ocean. Wang et al. (2019) used shipborne GNSS observations from a 20-day cruise in Fram Strait to investigate the accuracy of SARAL satellite PWV. Their result indicated a 1.7 kg/m² of RMSE between GNSS and SARAL PWV. One drawback in those studies is that both the area of evaluation region and the amount of statistical observations are limited due to the limitation of observing platform.

In this paper, the performance of Jason-3 AMR on a global scale was evaluated. In our experiment, the PWV derived from Jason-3 AMR are evaluated using the PWV from 103 globally distributed GNSS stations and 256 radiosonde stations that are distributed in islands or coastal areas. Compared with previous studies, we used many more and well distributed PWV observations from GNSS and radiosonde stations collected over a period of three years. Detailed and comprehensive comparison about the performance of Jason-3 AMR in island and coastal regions will be presented in following sections.

The rest of paper is organized as follows. First, the data used and PWV retrieving methods will be introduced in the section 2. Next, the method of PWV height correction will be introduced in section 3. Then, detailed discussion and analyses of five evaluation scenarios are shown in section 4. Finally, conclusions are summarized in section 5.

2 Data description and Methods

2.1 Jason-3 PWV

Jason-3 has a repeat period of around 9.9 days with 254 passes per cycle between latitude 66.15° S – 66.15° N. There are three families of Geophysical Data Records (GDR), i.e., Operational GDR, Interim GDR, and final GDR. The major differences among three products are their latency and quality. The final GDR products have the highest quality as it is generated using precise orbit, but it has the longest product latency (~ 60 days). In this work, Jason-3 ZWD with a sampling rate of 1 s from final GDR products is adopted. The Jason-3 ZWD values are then converted to PWV for comparison purpose. As an example, ZWD derived from Jason-3 cycle 1 is shown in Figure 1. Also, the integrity of Jason-3 GDR products from cycle 0 to cycle 119 is shown in Figure 2. It can be seen that all the data are complete except a small amount of data missing in a few cycles. It should be noted that the invalid observations flagged by land, sea ice and rain contamination have been excluded in this study. More detailed characteristics about Jason-3 can be found at (Maiwald et al., 2016).

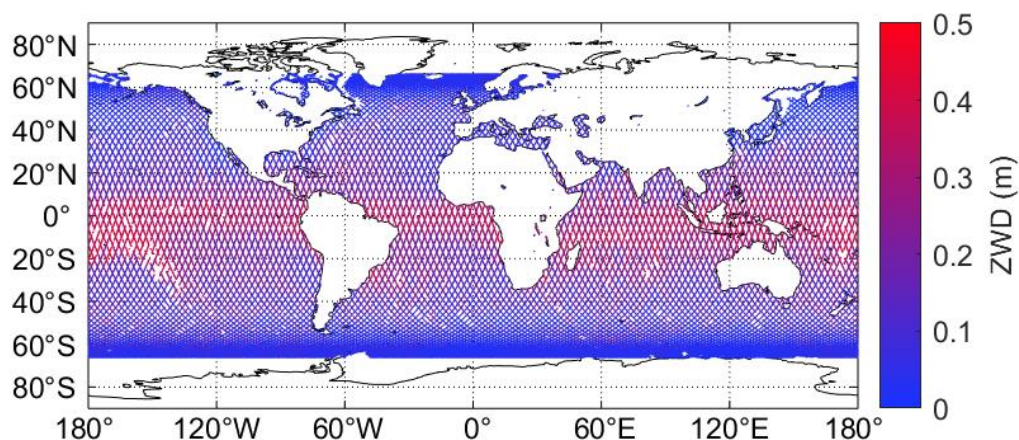


Figure 1. ZWD of Jason-3 satellite during its cycle 1 from 17 February 2016 to 27 February 2016.

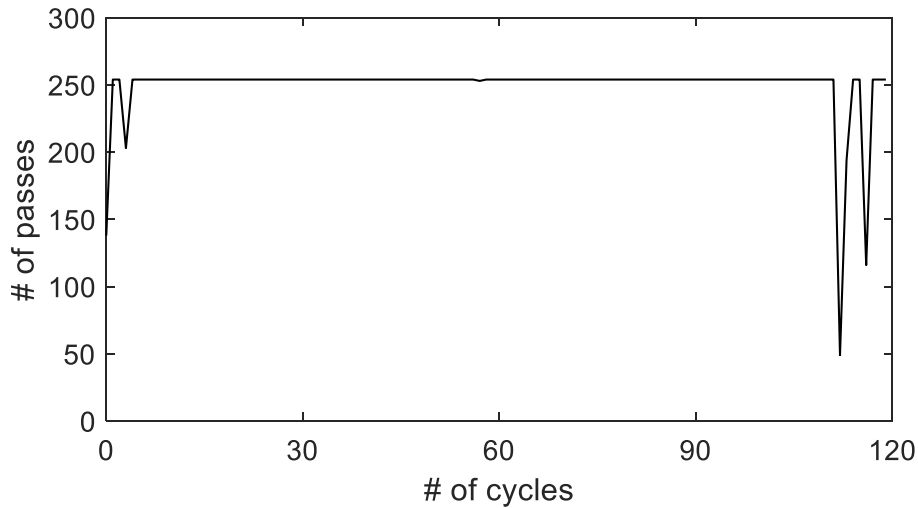


Figure 2. Integrity of Jason-3 final GDR products during cycles 0-119. There are 254 passes in a complete Jason-3 cycle.

2.2 Radiosonde PWV

Radiosonde is a traditional PWV observation system. It can measure meteorological parameters such as temperature, air pressure, and relative humidity at different altitudes over a radiosonde station. The PWV from radiosonde are normally treated as standard values to evaluate other PWV measurement techniques since it can achieve an accuracy of a few millimeters (Niell et al., 2001). However, because of its high operation cost, the temporal resolution of radiosonde data is low. Meteorological balloons are normally released just twice a day at UTC 0 and 12. A small number of stations also make radiosonde observations up to four times daily. Radiosonde data from 263 stations are used in this study. They are obtained from the Integrated Global Radiosonde Archive (IGRA) (<ftp://ftp.ncdc.noaa.gov/pub/data/igra>). The IGRA provides meteorological profiles for over 2,700 stations worldwide including ~1,000 active stations that are still in operation.

In this study, radiosonde PWV is selected to compare Jason-3 PWV according to the criterion: temporal separation of radiosonde and Jason-3 PWV observations is no more than 30 minutes; their spatial separation is no more than 100 km. Following this criterion, a total of 263 radiosonde stations have been selected from the IGRA dataset. Their distribution is shown in Figure 3.

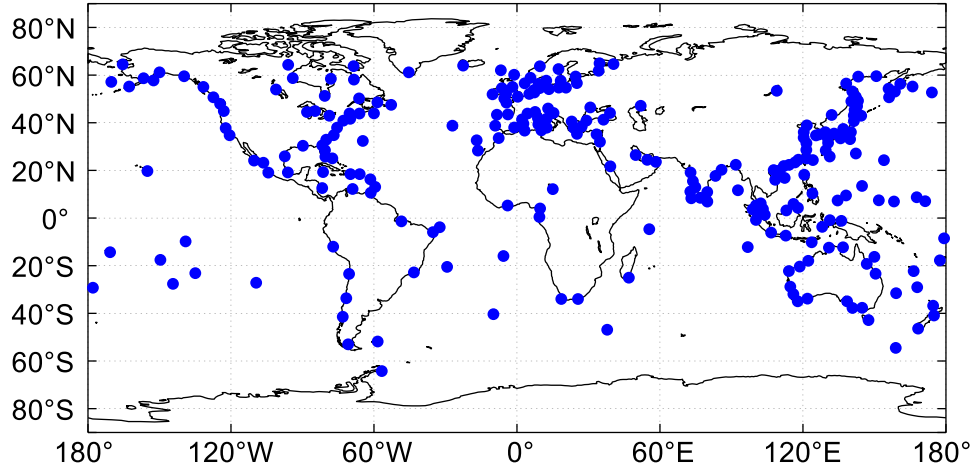


Figure 3. Distribution of 263 radiosonde stations used for PWV comparison with Jason-3 observations.

2.3 ECMWF PWV

By assimilating various observations from a variety of earth observation systems such as surface weather stations, ships, ocean buoys, radiosonde stations, and aircraft, ECMWF provides users with continuous, reliable, accurate meteorological grid products near the earth surface (Dee et al., 2011). In this study, the ECMWF ERA-Interim reanalysis grid product in pressure level is used. This grid product provides meteorological profiles i.e., temperature, relative humidity, pressure, at each grid point every 6 hours at UTC 0, 6, 12 and 18 since 1979 with a spatial resolution ranging from $0.125^\circ \times 0.125^\circ$ to $3^\circ \times 3^\circ$. Users can interpolate or extrapolate the meteorological parameters to any location near the earth surface. The spatial resolution of ECMWF ERA-Interim reanalysis product used in this study is $1^\circ \times 1^\circ$.

2.4 GNSS PWV

GNSS is a powerful geodetic technique to monitor PWV. The International GNSS Service (IGS) provides high quality, final tropospheric product Zenith Troposphere Delay (ZTD) for over 400 stations worldwide on a daily basis (Beutler et al., 1999). The temporal solution is as high as 5 minutes and its typical accuracy is 4 mm. In our study, the GNSS ZTD extracted from IGS products are interpolated to time point of Jason-3 PWV for comparison purpose. By a careful modeling and deduction of the zenith hydrostatic delay (ZHD) from GNSS ZTD, ZWD can be precisely obtained (Chen & Liu, 2016b). Subsequently PWV can be converted from ZWD using a PWV conversion factor (PWV_{factor}), i.e., $PWV = ZWD \times PWV_{\text{factor}}$. PWV_{factor} can be obtained based on local meteorological parameters i.e., temperature and air pressure.

Two approaches are applied in our study to calculate ZHD. One is to adopt the meteorological parameters from ECMWF products to calculate ZHD. It has been shown in China region that an accuracy of 2.8 mm for ECMWF ZHD (ZHD_{ECMWF}) can be obtained (Chen & Liu, 2016a). Another approach is to apply the widely used

empirical ZHD model, Saastamoinen model (Saastamoinen, 1972), to remove the ZHD. (Chen & Liu, 2016a) reported that ZHD from the Saastamoinen model (ZHD_{Saas}) has an accuracy of 8.4 mm in China region.

Similar to the criterion of selecting radiosonde PWV data, only GNSS stations within 100 km of Jason-3 footprints are selected for PWV comparison. With such a criterion, 103 IGS stations globally distributed in coastal and island areas are selected, as shown in Figure 4. As GNSS PWV has a high temporal resolution (5 min), GNSS PWV can be interpolated to every second of Jason-3 PWV observations.

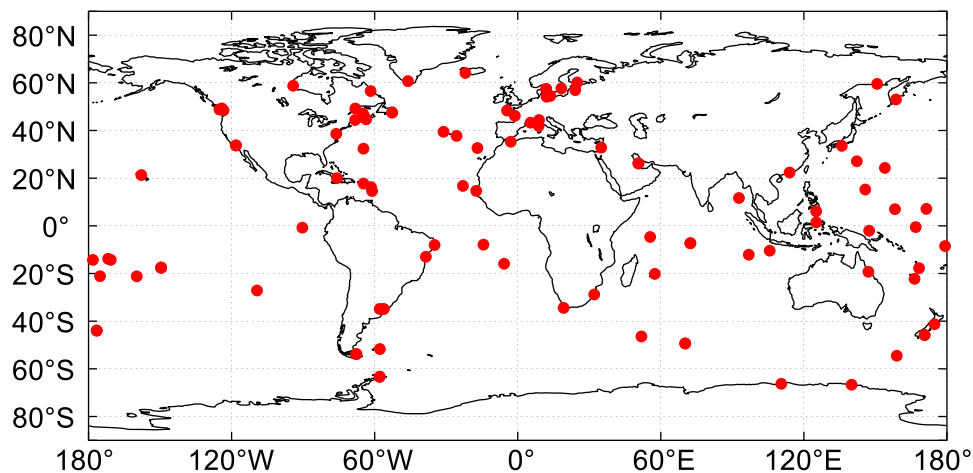


Figure 4. Globally distributed 103 GNSS stations in island and coastal regions are selected from the IGS network for PWV comparison.

3 PWV height correction

It should be noted that both radiosonde and GNSS PWV are referenced to their respective station heights while Jason-3 AMR PWV are referenced to the sea level. In order to assess the Jason-3 PWV, all PWV observations should be reduced to the same altitude. In this work, the sea level is selected as the reference altitude and all the PWV are referenced to sea level. Our results show that the amount of PWV between the sea level and height of one GNSS station (22.24° N, 116.42° E, orthometric height 100 m) can be up to 2.2 kg/m² and apparently the PWV height correction for radiosonde and GNSS PWV data is not negligible.

The reduction of the radiosonde PWV to sea level is relatively straightforward. By interpolating or extrapolating the meteorological parameters recorded by the radiosonde station itself, the PWV between station height and sea level can be calculated. It can then be used to reduce the radiosonde PWV to the sea level.

For GNSS PWV, the PWV reduction is relatively complex and two methods are studied in this study, as shown below. The first method, denoted as Kouba method, is to use the empirical equation (Kouba, 2008):

$$PWV_{hs} = PWV_{h0} \cdot e^{\frac{h0-hs}{2000}} \quad (1)$$

where PWV_{hs} and PWV_{h0} correspond to PWV at the elevation of station (h_s , unit: m) and sea level (h_0 , 0 m in this study), respectively. It has been shown that this empirical equation can introduce 28% and 5% of PWV differences when the heights

of station are 500 m and 100 m, respectively (Fernandes et al., 2015). To minimize PWV contamination resulting from height correction, only those radiosonde and GNSS stations that have an orthometric height below 500 m are adopted in this study. A statistic of the orthometric heights of radiosonde and GNSS stations are shown in Table 2. It should be noted that a few stations have a height in the range of -100 m to 0 m. Their absolute height values are used in the calculation of average height.

The second method, denoted as ECMWF method, is to interpolate or extrapolate the meteorological parameters, which are obtained from ECMWF ERA-Interim reanalysis products, for both the sea level and the height of GNSS station. The PWV between the station height and sea level can be calculated using the meteorological profiles. This PWV will be used to reduce the GNSS PWV from their station heights to sea level.

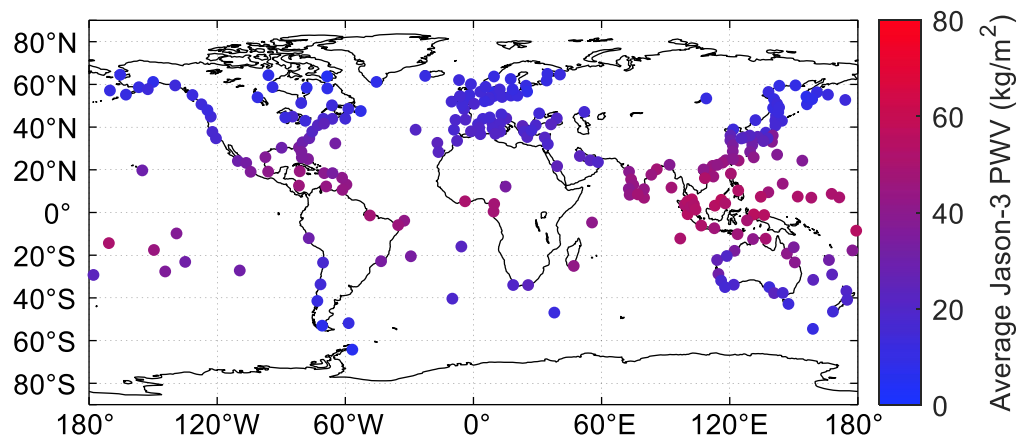
Table 2 A statistic of radiosonde and GNSS station orthometric heights.

Height range	Radiosonde		GNSS	
	# of stations	Average height (m)	# of stations	Average height (m)
-100 m – 100 m	234	27	91	29
100 m – 200 m	18	129	6	127
200 m – 500 m	11	331	6	343
< 500 m	263	47	103	53

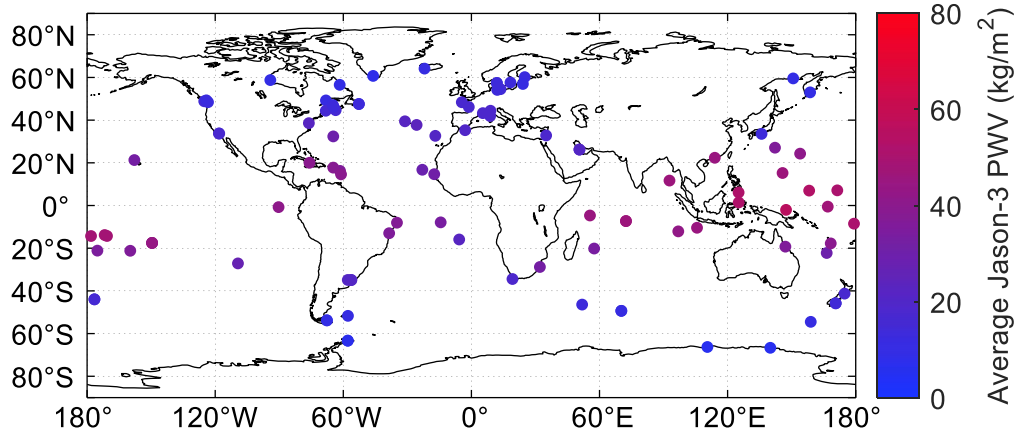
4 Results and analyses

4.1 Jason-3 average PWV at GNSS and radiosonde stations

The Jason-3 PWV values, observed with an interval of 1 second at crossover points collocated with every radiosonde/GNSS station, are depicted in Figure 5. Figure 5(a) and (b) show that the PWV values in the low latitudes are much higher than those in the high latitudes. This is because of the high level of humidity in the equatorial region.



(a) Average Jason-3 PWV at every radiosonde station.



(b) Average Jason-3 PWV at every GNSS station.

Figure 5. Average Jason-3 PWV at radiosonde/GNSS stations during Jason-3 cycle 0 – cycle 119 (12 February 2016 - 12 May 2019).

4.2 Reducing radiosonde and GNSS PWV to sea level

Both radiosonde PWV and GNSS PWV are used to evaluate the accuracy of the Jason-3 PWV. The calculation of radiosonde PWV is straightforward and it is directly calculated from the meteorological parameters observed at each radiosonde station. To reduce the PWV from radiosonde height to sea level, meteorological parameters from radiosonde are interpolated or extrapolated first and they are then used to calculate the amount of PWV reduction.

For the calculation of GNSS PWV, four different schemes are studied to correct the zenith hydrostatic delay and the reduction of PWV from GNSS station height to sea level, as illustrated in Table 3. They are: (1) in the first scheme, the ZHD is estimated using the ECMWF model and the Kouba method is used to reduce the PWV effect of GNSS station height to sea level; (2) the second scheme is similar to the first one but the ECMWF method is used to reduce the PWV effect of GNSS station height to sea level; (3) in the third scheme, the ZHD is estimated using the Saastamoinen model and the Kouba method is used to reduce the PWV effect of GNSS station height to sea level; (4) the fourth scheme is very similar to the third scheme but the ECMWF method is used to reduce the PWV effect of GNSS station height to sea level.

Table 3 The schemes of reducing GNSS PWV from station height to sea level

Scheme	Estimation of PWV	Method of reducing the PWV effect of GNSS station height to sea level
1	$(ZTD_{GNSS} - ZHD_{ECMWF}) \times PWV_{factor}$	Kouba method
2	$(ZTD_{GNSS} - ZHD_{ECMWF}) \times PWV_{factor}$	ECMWF method
3	$(ZTD_{GNSS} - ZHD_{Saas}) \times PWV_{factor}$	Kouba method
4	$(ZTD_{GNSS} - ZHD_{Saas}) \times PWV_{factor}$	ECMWF method

4.3 Data quality control strategy

In order to obtain reliable comparison results, the quality of the PWV data should be

controlled carefully. The algorithm error of deriving ZWD from OSTM/Jason-2 Advanced Microwave Radiometer data is <15 mm in coastal regions (Brown, 2010). We assume that the magnitude of ZWD error from Jason-3 data is similar in this study. The uncertainty of final IGS ZTD products is around 4 mm (Li et al., 2012). In this study, we consider the accuracies of ZHD_{ECMWF} and ZHD_{Saas} as 2.8 mm and 8.4 mm, respectively (Chen & Liu, 2016a). According to the error propagation law, the theoretical accuracies of ZWD differences between GNSS and Jason-3, i.e., $(ZTD_{GNSS} - ZHD_{ECMWF} - ZWD_{Jason-3})$ and $(ZTD_{GNSS} - ZHD_{Saas} - ZWD_{Jason-3})$ are about 16 mm and 18 mm (around 2.7 kg/m² and 3.0 kg/m² in PWV), respectively. The accuracy of PWV difference between radiosonde and Jason-3 should be higher due to the higher accuracy of radiosonde PWV. Considering the spatial and temporal separation of two sets of PWV data as well as the error from station height PWV reduction, 10 kg/m² is defined as the threshold to detect outliers in PWV differences based on the 3 σ rule. This means that those pairs of PWV comparisons larger than 10 kg/m² are regarded as outliers and excluded in this study.

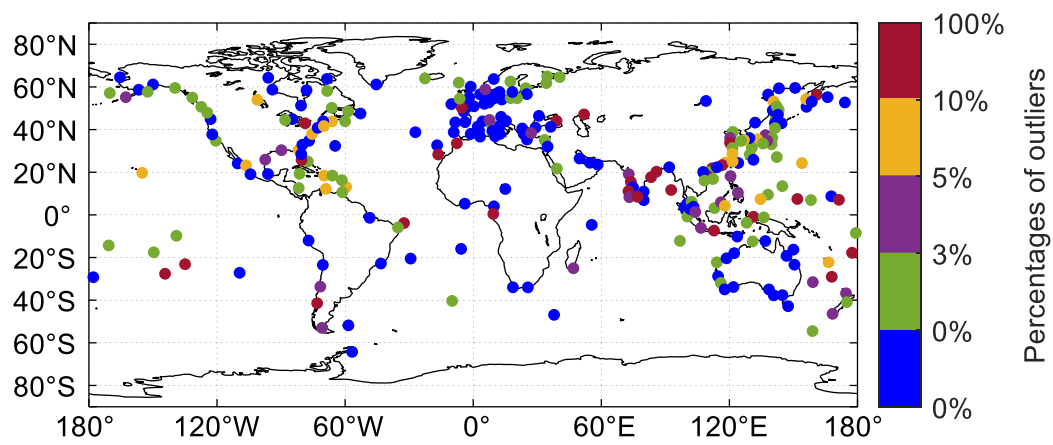
The numbers of total PWV observations and outliers are shown in Table 4. It shows that only 2.7% of radiosonde PWV data are outliers. For the GNSS PWV data, the percentages of outliers are different depending on the scheme of ZHD calculation model and PWV reduction method. The scheme 1 has the highest outlier percentage of 2.0% and the scheme 4 has the lowest percentage of 0.8%. In schemes 3 and 4, the Saastamoinen model is used to calculate the zenith hydrostatic delay and their outlier percentages are lower than schemes 1 and 2 where the ECMWF model is used. Our explanation is that the IGS community normally uses the Saastamoinen model in the GNSS data analysis. Therefore the use of Saastamoinen model to remove the ZHD in this study is consistent with the IGS practice and this appears to produce a better result.

Table 4 The statistics of radiosonde and GNSS PWV data points according to different latitude regions. The percentage denotes the number of outliers out of the total number of PWV observations.

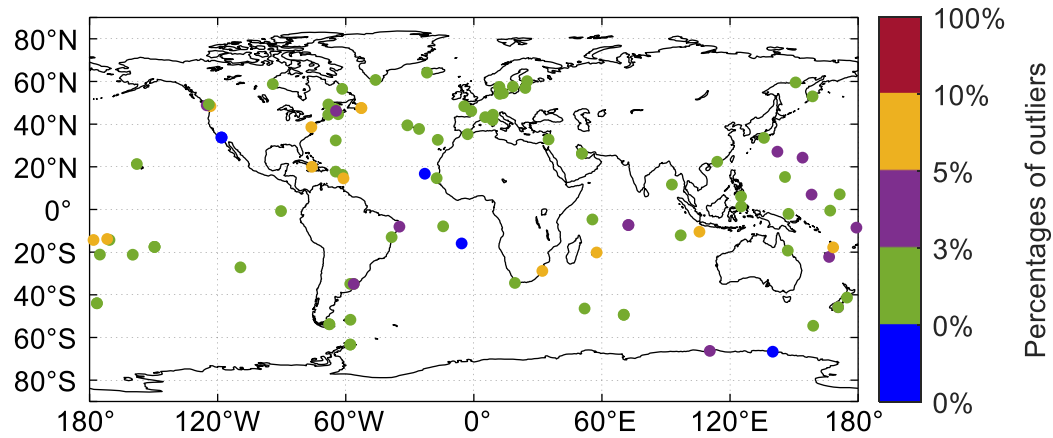
Latitude regions	Radiosonde		GNSS				
	# of PWV observations	# of PWV outliers	# of PWV observations	# of PWV outliers			
			Scheme 1-4	Scheme 1	Scheme 2	Scheme 3	Scheme 4
20° S–20° N	13655	603 (1%)	106634	2907 (0.8%)	2494 (0.7%)	1426 (0.4%)	1265 (0.3%)
20°–40° N and 20°–40° S	18013	597 (1%)	77922	1767 (0.5%)	1422 (0.4%)	1105 (0.3%)	941 (0.2%)
40°–70° N and 40°–70° S	30748	428 (0.7%)	197008	2847 (0.7%)	2519 (0.7%)	1238 (0.3%)	1081 (0.3%)
Global	62416	1628 (2.7%)	381564	7521 (2.0%)	6435 (1.8%)	3769 (1.0%)	3287 (0.8%)

The percentage of the PWV data outliers at each radiosonde and GNSS station is

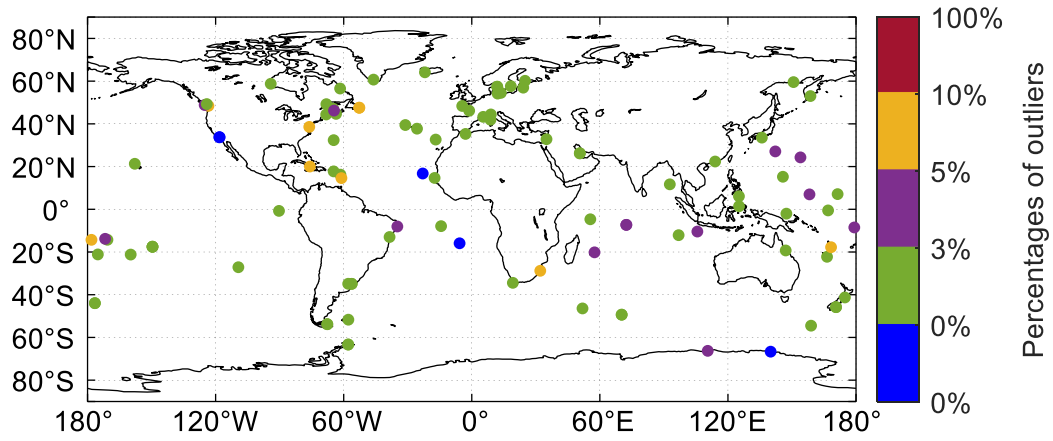
shown in Figure 6. Evidently, for most radiosonde/GNSS stations, the outlier percentage is no more than 3%. Stations with relatively high percentages of outliers are generally located in the low latitude region. This is probably because the humidity level in the low latitudes is high and the discrepancy between two types of PWV dataset more likely exceeds the 3σ criterion. The statistical results are also reported in Table 5. For radiosonde station, 123 radiosonde stations are free of outlier. Among the remaining 140 radiosonde stations, 48% of them (67) have outliers less than 3% and 29 stations have outliers more than 10%. For GNSS stations, 5 to 11 stations are free of outliers, depending on the selection of scheme. 73 to 83 GNSS stations have outliers no more than 3% in the four GNSS schemes.



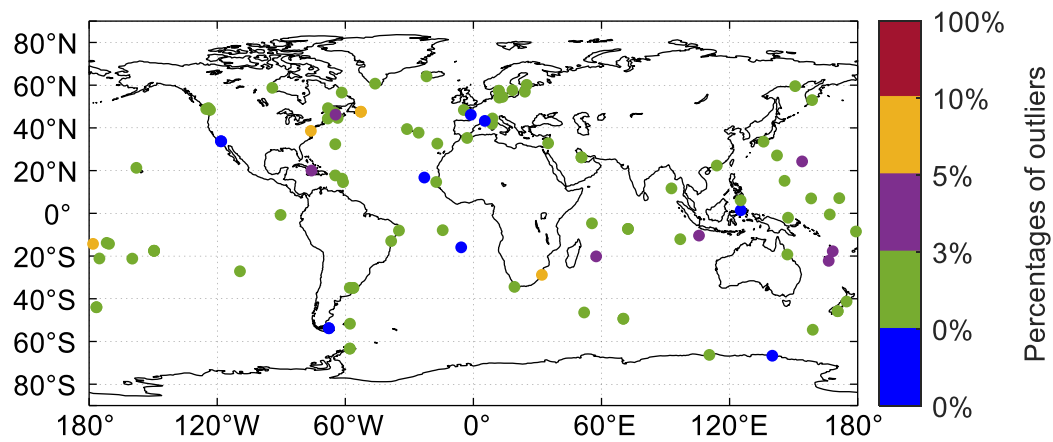
(a) The percentage of PWV data outliers at every radiosonde station



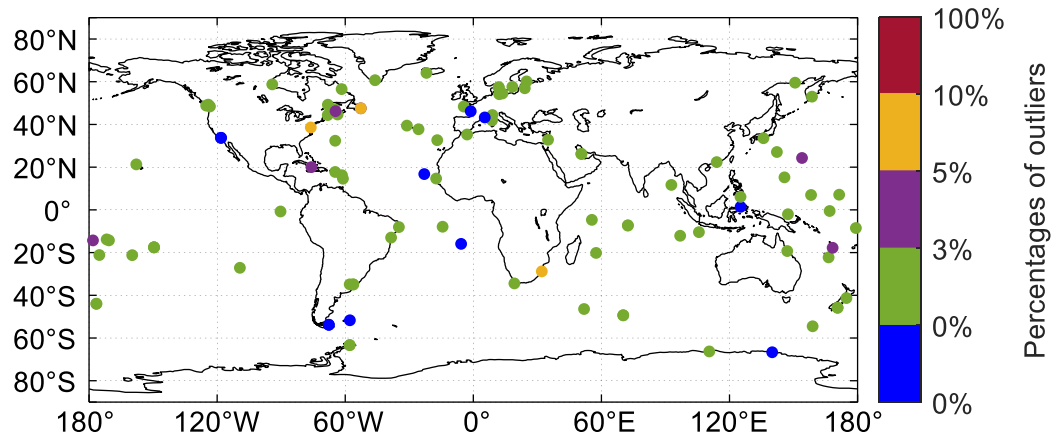
(b) The percentage of PWV data outliers at every GNSS station in scheme 1



(c) The percentage of PWV data outliers at every GNSS station in scheme 2



(d) The percentage of PWV data outliers at every GNSS station in scheme 3



(e) The percentage of PWV data outliers at every GNSS station in scheme 4

Figure 6. The percentages of PWV data outliers at every radiosonde/GNSS station.

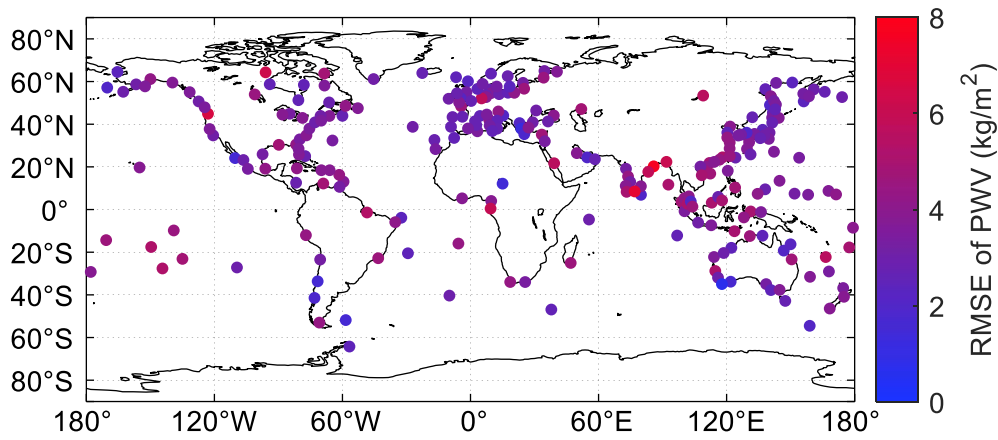
Table 5 Statistics of radiosonde and GNSS stations in each level of outlier percentage.

Percentages of outliers	Number of radiosonde stations	Number of GNSS stations			
		Scheme 1	Scheme 2	Scheme 3	Scheme 4
0%	123	5	5	10	11
(0% - 3%]	67	73	76	81	83

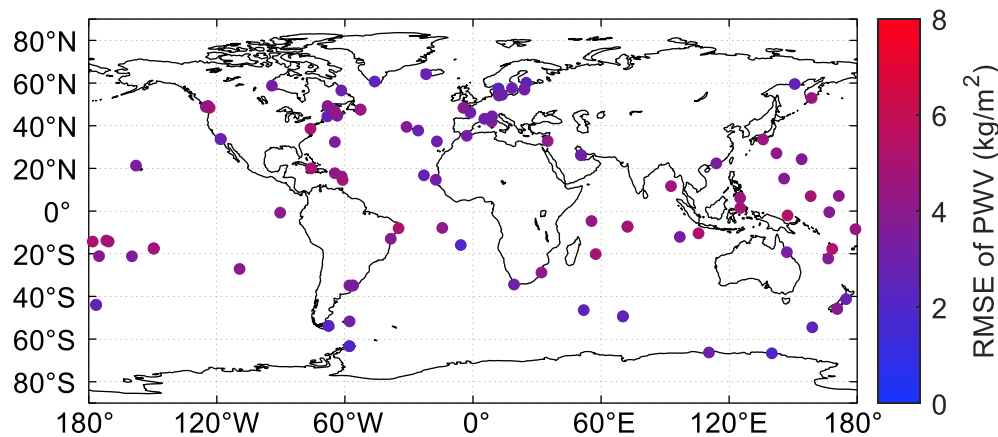
(3% -5%]	22	13	13	7	6
(5% - 10%]	22	12	9	5	3
(10% - 100%]	29	0	0	0	0
[0% - 100%]	263	103	103	103	103

4.4 Spatial assessment of Jason-3 PWV using radiosonde and GNSS PWV

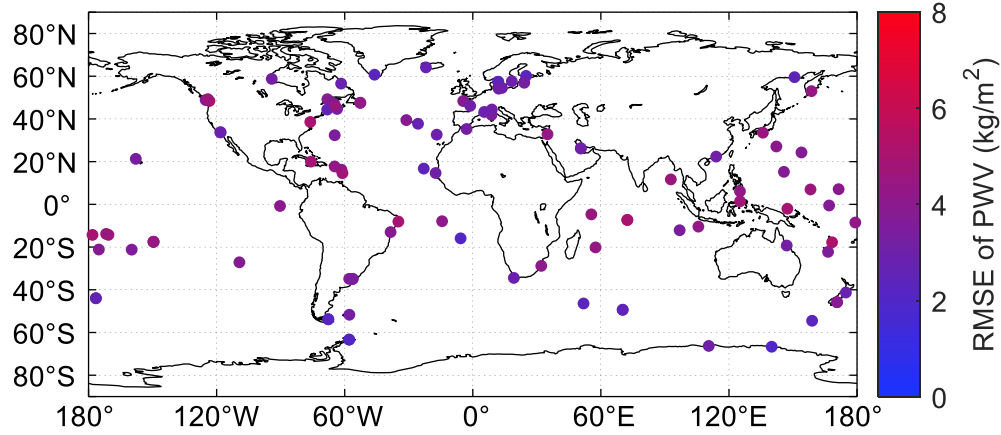
The accuracy of Jason-3 PWV is evaluated using both radiosonde and GNSS PWV data. Both radiosonde and GNSS PWV have been reduced from their station heights to the sea level according to the approach in section 4.2. Figure 7 shows the PWV RMSE of Jason-3 at 263 radiosonde stations and 103 GNSS stations over a period of more than 3 years from cycle 0 to cycle 119 (12 February 2016 to 12 May 2019). It is evident that most radiosonde and GNSS stations have a good agreement with Jason-3 PWV, although a few stations in the low latitude region have large RMSE. The percentages of radiosonde and GNSS stations for different PWV RMSE thresholds are shown in Figure 8. It can be seen that more than 70% of radiosonde stations have a PWV RMSE less than 4 kg/m^2 . The use of ZHD_{Saas} correction (schemes 3-4) in GNSS PWV has a better agreement with Jason-3 PWV than the use of $\text{ZHD}_{\text{ECMWF}}$ correction (schemes 1-2). Around 90% of GNSS stations with schemes 3-4 have a PWV RMSE less than 4 kg/m^2 , while only around 65% of GNSS stations with schemes 1-2 have a PWV RMSE less than 4 kg/m^2 .



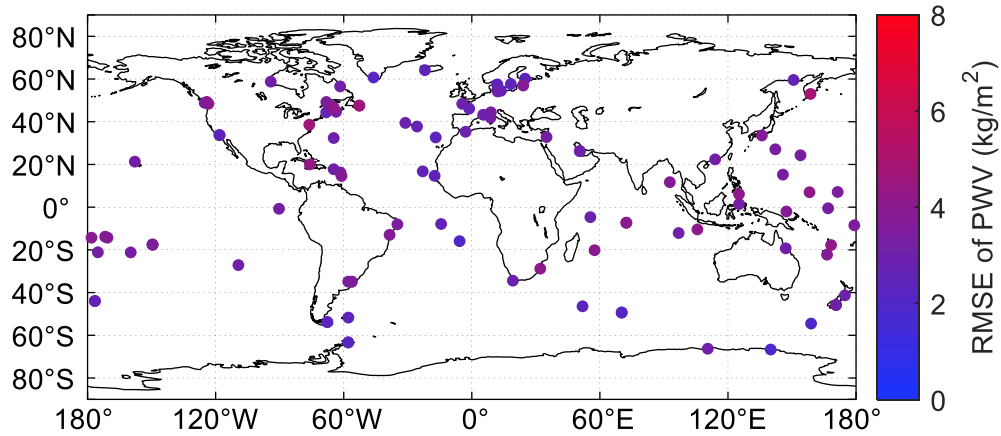
(a) PWV RMSE between 263 radiosonde stations and Jason-3



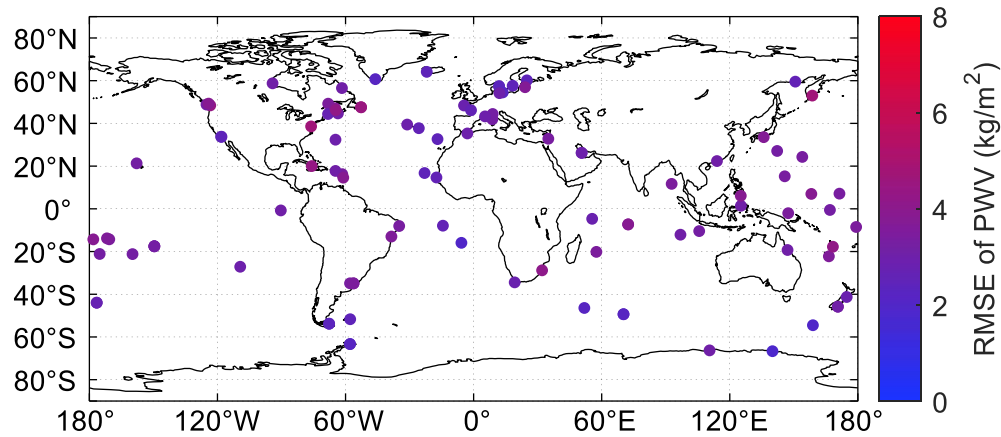
(b) PWV RMSE between 103 GNSS stations and Jason-3. The scheme 1 is used to reduce the PWV effect of GNSS station height to sea level.



(c) PWV RMSE between 103 GNSS stations and Jason-3. The scheme 2 is used to reduce the PWV effect of GNSS station height to sea level.



(d) PWV RMSE between 103 GNSS stations and Jason-3. The scheme 3 is used to reduce the PWV effect of GNSS station height to sea level.



(e) PWV RMSE between 103 GNSS stations and Jason-3. The scheme 4 is used to reduce the PWV effect of GNSS station height to sea level.

Figure 7. RMSE between Jason-3 PWV and PWV from 263 radiosonde stations and 103 GNSS stations during Jason-3 cycles 0–119 (12 February 2016–12 May 2019).

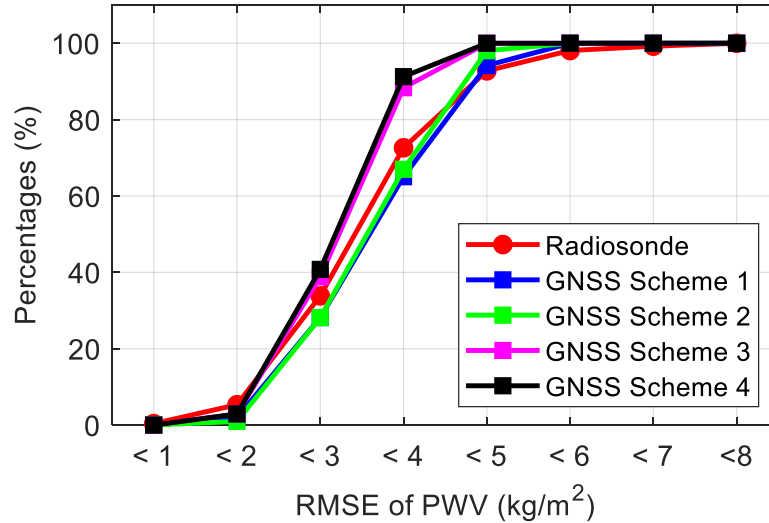


Figure 8. The percentages of radiosonde and GNSS stations under different levels of PWV RMSE and different schemes.

4.5 RMSE of Jason-3 PWV data with respect to distance to land

In the Jason-3 GDR products, the radial distance from Jason-3 footprint to coastal land is also provided. The effect of such a radial distance on The PWV RMSE is studied on the basis of classification of their different values of radial distance: < 5 km, 5–10 km, 10–15 km, 15–20 km, 20–50 km, 50–100 km. As shown in Figure 9, Jason-3 PWV evaluated using GNSS PWV with scheme 4 has the smallest RMSE, only the GNSS scheme 4 results are shown (Figure 9 (b), (d), (f)). It is noted that 3,177 radiosonde and 18,551 GNSS PWV comparison points are not included in the statistic because the radial distance exceeds 100 km for their radiosonde/GNSS stations.

It is found that the RMSE of Jason-3 PWV generally decreases as the radial distance increases. This is true in different latitude regions except the results evaluated by GNSS PWV in latitude 20°–40° S/N (Figure 9 (d)). For instance, the Jason-3 PWV RMSE evaluated by the radiosonde at 40°–70° S/N decreases from 3.4 kg/m² to 2.7 kg/m² when the radial distance increases from <5 km to 50–100 km. Similarly, a decrease from approximately 3.0 kg/m² to 2.5 kg/m² is also observed with the results evaluated by GNSS PWV at 40°–70° S/N. One exception is shown in case of Figure 9(d). where the radial distance is < 5 km, the Jason-3 RMSE is actually smaller than the RMSE results that correspond to radial distance larger than 5 km. This is because the Jason-3 footprints are also very close to GNSS stations (approximately 40 km). The short separation between Jason-3 and GNSS stations explains the good agreement between Jason-3 and GNSS PWV in the < 5 km category.

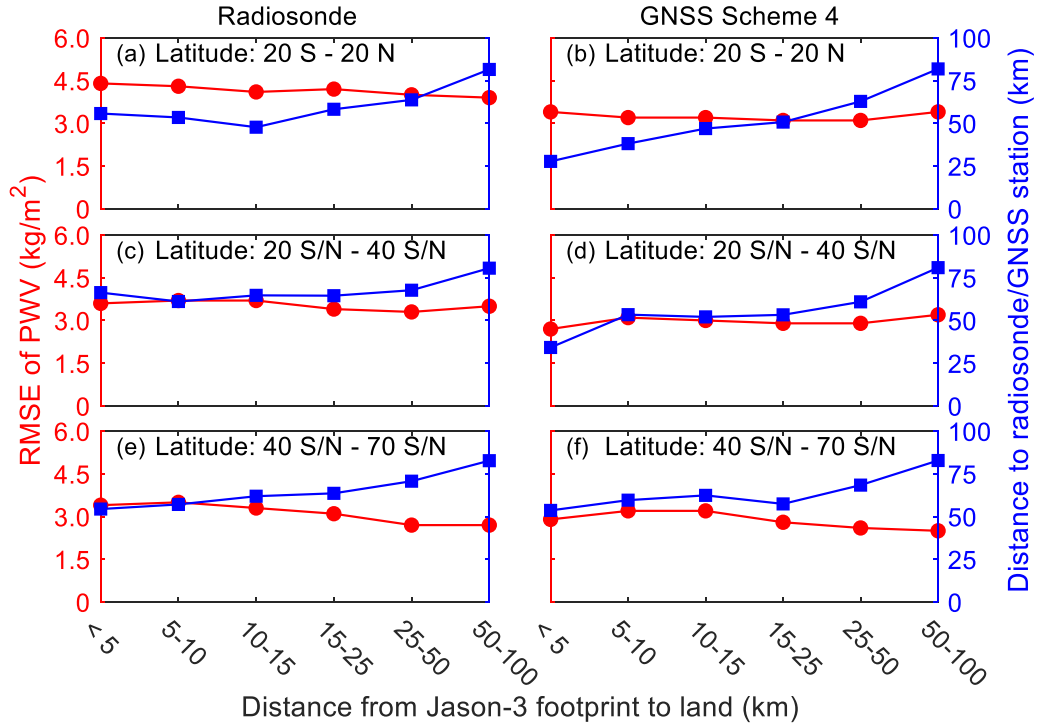


Figure 9. The relationship between PWV RMSE and latitude and distance from Jason-3 footprints to land.

4.6 RMSE of Jason-3 PWV data with respect to latitude

It is also found that the RMSE generally decreases with the increase of latitude, as shown in Table 6. The Jason-3 PWV RMSE evaluated by radiosonde PWV are 4.0 kg/m², 3.5 kg/m², and 3.0 kg/m² at latitudes 20° S–20° N, 20° S/N–40° S/N, and 40° S/N–70° S/N, respectively. Correspondingly the Jason-3 PWV RMSE evaluated by GNSS PWV (scheme 4) are 3.3 kg/m², 3.1 kg/m², and 2.8 kg/m² at latitudes 20° S–20° N, 20° S/N–40° S/N, and 40° S/N–70° S/N, respectively.

Table 6 RMSE and average (in the parentheses) of PWV difference of Jason-3 in comparison with radiosonde as well as GNSS at different latitude regions during the Jason-3 cycles 0 – 119 (unit: kg/m²).

Latitude regions	Radiosonde PWV	GNSS PWV			
		Scheme 1	Scheme 2	Scheme 3	Scheme 4
20° S – 20° N	4.0 (3.3)	4.3 (3.6)	4.2 (3.5)	3.4 (2.7)	3.3 (2.6)
20° – 40° S and 20° – 40° N	3.5 (2.7)	3.6 (2.9)	3.5 (2.8)	3.1 (2.4)	3.1 (2.4)
40° – 70° S and 40° – 70° N	3.0 (2.3)	3.0 (2.3)	3.0 (2.3)	2.8 (2.2)	2.8 (2.2)
Global	3.4 (2.6)	3.5 (2.8)	3.5 (2.7)	3.1 (2.4)	3.0 (2.3)

The radiosonde in theory has the ability to measure PWV with an accuracy of 1-2 kg/m² (Niell et al., 2001). The accuracy of Jason-3 PWV is ~2.5 kg/m² at coastlines, as discussed before. Thus the RMSE of Jason-3 PWV when evaluated by radiosonde is estimated to be ~3.0 kg/m². Considering the fact that the radiosonde station might not be exactly collocated with the Jason-3 footprints (spatial separation

up to 100 km) and the radiosonde PWV might not be synchronously observed with Jason-3 PWV data (temporal separation up to 30 minutes), the 3.4 kg/m² RMSE of Jason-3 PWV using 263 global radiosonde stations is considered reasonable in this study.

As discussed in previous sections, the PWV RMSE of GNSS is ~3.0 kg/m² if using the Saastamoinen model to correct the ZHD delay in the IGS zenith tropospheric delay. Considering that the GNSS station spatial separation from the Jason-3 footprints (up to 100 km) and that the error resulting from GNSS station height reduction to sea level, we think the RMSE of 3.1 kg/m² and 3.0 kg/m² shown in **Error! Reference source not found.** for schemes 3 and 4, respectively, are reasonable.

Jason-3 PWV assessed by GNSS PWV using schemes 1 and 2 (ZHD corrected by ECMWF model, ZHD_{ECMWF}) has a larger RMSE (3.5 kg/m²) when compared to schemes 3 and 4. Though previous study showed that ZHD_{ECMWF} has a better accuracy than Saastamoinen and other models (Chen & Liu, 2016a). The reason is that the Saastamoinen model is routinely adopted by IGS data analysis centers to model ZHD. Therefore, using Saastamoinen model in this study to remove ZHD from the IGS products can get a more self-consistent PWV.

4.7 Seasonal variation of RMSE of Jason-3 PWV data

Figure 10 presents the monthly Jason-3 PWV RMSE evaluated with radiosonde and GNSS PWV during the entire 39-month period. It is evident that the PWV accuracy show a strong season variation. All the monthly RMSE values become more significant in the summer months (north hemisphere) than winter months. This is particularly event in the radiosonde evaluation results. In the GNSS evaluation results, the seasonal variation in the results using schemes 1 and 2 is more evident than those using schemes 3 and 4.

The monthly RMSE of Jason-3 PWV evaluated using radiosonde PWV exhibits the most significant monthly variation, varying from 2.5 kg/m² to 4.1 kg/m². Jason-3 PWV evaluated with GNSS schemes 3 and 4 has the smallest monthly RMSE value. The monthly RMSE largely fluctuates around 3.0 kg/m². Compared with GNSS PWV schemes 3 and 4, the RMSE of Jason-3 PWV using GNSS PWV schemes 1 and 2 are larger by 0.4-0.5 kg/m².

As shown in Figure 3 most of radiosonde stations are located in the northern hemisphere. In the summer months the magnitude of PWV is much larger than that in winter. Owing to the large variability of water vapor, the RMSE of PWV in the summer months is consequently larger in summer months. In comparison, the GNSS stations have a better distribution in both north and south hemisphere, as shown in Figure 4. This explains that the summer and winter RMSE of Jason-3 evaluated using GNSS PWV demonstrate a less significant monthly variation, particularly for the schemes 3 and 4.

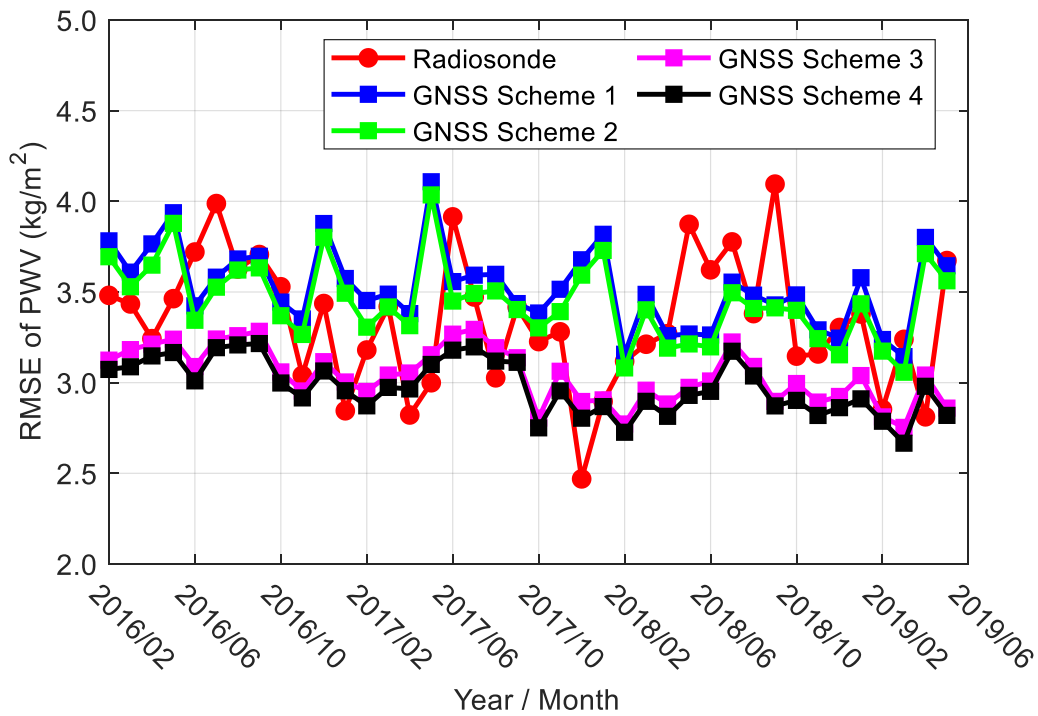
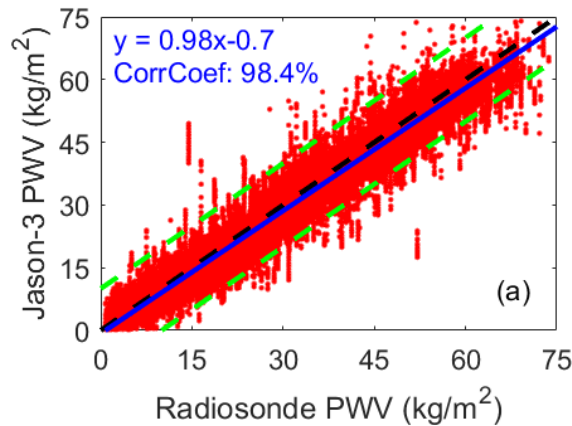


Figure 10. Time series of monthly RMSE of Jason-3 PWV data in comparison with radiosonde and GNSS PWV during Jason-3 cycles 0–119 (12 February 2016–12 May 2019).

4.8 Correlation between Jason-3 PWV and radiosonde/GNSS PWV

To further investigate the agreement between Jason-3 PWV and radiosonde and GNSS PWV, the correlations between the three sets of PWV data are shown in Figure 11. As shown in Figure 11(a), the correlation coefficients between Jason-3 and radiosonde PWV is 0.984. PWV calculated from four GNSS schemes all show a good agreement with Jason-3 PWV. The correlation coefficients of the schemes 1 to 4 are all 0.988.



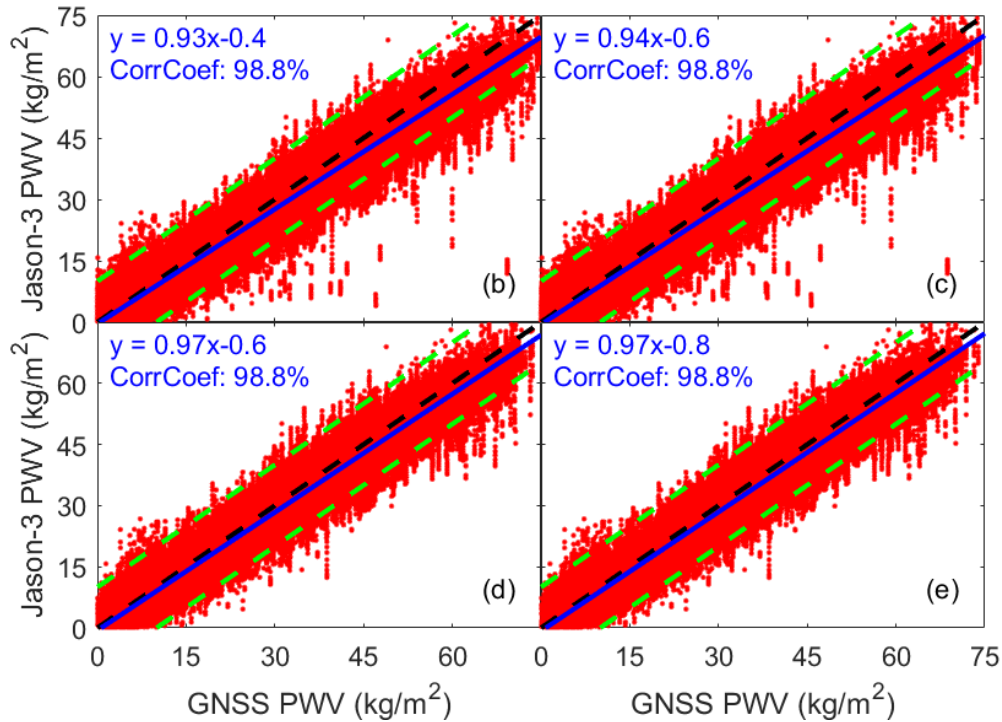


Figure 11. Scatter plot of radiosonde and GNSS PWV against Jason-3 PWV during Jason-3 cycle 0 - cycle 119. Blue line is the fitting result. The black dashed line is $y = x$. The green dashed lines are the threshold lines (10 kg/m^2): $y = x \pm 10$. (a) radiosonde, (b)GNSS PWV using correction scheme 1, (c) GNSS PWV using correction scheme 2, (d) GNSS PWV using correction scheme 3, (e) GNSS PWV using correction scheme 4.

5 Conclusions

Jason-3 is a relatively new altimetry satellite mission. A comprehensive assessment of its PWV at a global scale with multiple years of data is needed in order to fully understand its performance and capability. We used global PWV from 263 radiosonde stations and 103 GNSS stations, all of which are located in islands and coastal regions, to evaluate the Jason-3 PWV during its flight cycle 0 to cycle 119 (12 February 2016 - 12 May 2019). Over 60,000 radiosonde PWV comparison points and over 380,000 GNSS PWV comparison points are used in this study. The percentages of outliers in radiosonde PWV and GNSS PWV data are 2.7% and 0.8%-2.0%, respectively. The outliers are discarded based on our data quality control criterion: PWV difference not exceeding 10 kg/m^2 .

The accuracy of Jason-3 PWV is very consistent when evaluated by either radiosonde or GNSS. Globally the RMSE of Jason-3 PWV data is 3.4 kg/m^2 when compared to radiosonde PWV. The global RMSE is in the range of $3.0 - 3.5 \text{ kg/m}^2$ for four GNSS PWV processing schemes. Four schemes are proposed to calculate the GNSS PWV and we find that the scheme 4, i.e. the combined use of Saastamoinen model to remove the ZHD and the ECMWF model to reduce the PWV from GNSS station height to sea level, is the best option (RMSE 3.0 kg/m^2). This is because the IGS community also uses the Saastamoinen model in the generation of IGS zenith tropospheric delay products.

The RMSE of Jason-3 PWV increases when the Jason-3 footprints are closer to the land. The RMSE increases as the latitude decreases. The RMSE of Jason-3 PWV show evident seasonal variation, the RMSE in summer season (north hemisphere) larger than winter season. Both radiosonde and GNSS PWV have a high correlation with the Jason-3 PWV data with correlation coefficient of 0.984-0.988.

Acknowledgment

The support from the Key Program of the National Natural Science Foundation of China (No. 41730109) is acknowledged. The supports by the Hong Kong Research Grants Council (RGC) (No. B-Q52W PolyU 152149/16E and B-Q61L PolyU 152222/17E) are acknowledged. The Emerging Frontier Area (EFA) Scheme of Research Institute for Sustainable Urban Development (RISUD) of the Hong Kong Polytechnic University (No. 1-BBWJ) is also acknowledged. We want to thank Centre National d'Études Spatiales (CNES) AVISO archives for providing the Jason-3 GDR data (<ftp://ftp-access.aviso.altimetry.fr/geophysical-data-record/>). The National Oceanic and Atmospheric Administration (NOAA) is thanked for providing the IGRA radiosonde data (<ftp://ftp.ncdc.noaa.gov/pub/data/igra/>). The European Centre for Medium-Range Weather Forecasts is appreciated for providing the ECMWF reanalysis data (<https://apps.ecmwf.int/datasets/data/interim-full-daily/levtype=pl/>). The authors also want to thank the IGS for providing the GNSS ZTD products (<ftp://cddis.gsfc.nasa.gov/gps/products/troposphere/zpd/>).

References

- Ablain, M., Philipps, S., Picot, N., & Bronner, E. (2010). Jason-2 Global Statistical Assessment and Cross-Calibration with Jason-1. *Marine Geodesy*, 33(sup1), 162–185. <https://doi.org/10.1080/01490419.2010.487805>
- Beutler, G., Rothacher, M., Schaer, S., Springer, T., Kouba, J., & Neilan, R. (1999). The International GPS Service (IGS): an interdisciplinary service in support of earth sciences. *Advances in Space Research*, 23(4), 631–653.
- Brown, S. (2010). A Novel Near-Land Radiometer Wet Path-Delay Retrieval Algorithm: Application to the Jason-2/OSTM Advanced Microwave Radiometer. *IEEE Transactions on Geoscience and Remote Sensing*, 48(4), 1986–1992. <https://doi.org/10.1109/TGRS.2009.2037220>
- Brown, S., Ruf, C., Keihm, S., & Kitiyakara, A. (2004). Jason Microwave Radiometer Performance and On-Orbit Calibration. *Marine Geodesy*, 27(1–2), 199–220. <https://doi.org/10.1080/01490410490465643>
- Chambers, D. P., Ries, J. C., & Urban, T. J. (2003). Calibration and Verification of Jason-1 Using Global Along-Track Residuals with TOPEX Special Issue: Jason-1 Calibration/Validation. *Marine Geodesy*, 26(3–4), 305–317. <https://doi.org/10.1080/714044523>
- Chen, B., & Liu, Z. (2016a). A Comprehensive Evaluation and Analysis of the Performance of Multiple Tropospheric Models in China Region. *IEEE Transactions on Geoscience and Remote Sensing*, 54(2), 663–678.

<https://doi.org/10.1109/TGRS.2015.2456099>
 Chen, B., & Liu, Z. (2016b). Global water vapor variability and trend from the latest
 36 year (1979 to 2014) data of ECMWF and NCEP reanalyses, radiosonde,
 GPS, and microwave satellite. *Journal of Geophysical Research: Atmospheres*,
 121(19), 11,442–11,462. <https://doi.org/10.1002/2016JD024917>
 Dee, D. P., Uppala, S. M., Simmons, A. J., Berrisford, P., Poli, P., Kobayashi, S., et al.
 (2011). The ERA-Interim reanalysis: configuration and performance of the
 data assimilation system. *Quarterly Journal of the Royal Meteorological
 Society*, 137(656), 553–597. <https://doi.org/10.1002/qj.828>
 Fernandes, M. J., Lázaro, C., Ablain, M., & Pires, N. (2015). Improved wet path
 delays for all ESA and reference altimetric missions. *Remote Sensing of
 Environment*, 169, 50–74. <https://doi.org/10.1016/j.rse.2015.07.023>
 Fernandes, M. J., Lázaro, C., Nunes, A. L., Pires, N., Bastos, L., & Mendes, V. B.
 (2010). GNSS-Derived Path Delay: An Approach to Compute the Wet
 Tropospheric Correction for Coastal Altimetry. *IEEE Geoscience and Remote
 Sensing Letters*, 7(3), 596–600. <https://doi.org/10.1109/LGRS.2010.2042425>
 Fernandes, M. J., & Lázaro, C. (2018). Independent assessment of sentinel-3A wet
 tropospheric correction over the open and coastal ocean. *Remote Sensing*,
 10(3), 484.
 Haines, B. J., Dong, D., Born, G. H., & Gill, S. K. (2003). The Harvest Experiment:
 Monitoring Jason-1 and TOPEX/POSEIDON from a California Offshore
 Platform Special Issue: Jason-1 Calibration/Validation. *Marine Geodesy*,
 26(3–4), 239–259. <https://doi.org/10.1080/714044520>
 Keihm, S. J., Zlotnicki, V., & Ruf, C. S. (2000). TOPEX microwave radiometer
 performance evaluation, 1992–1998. *IEEE Transactions on Geoscience and
 Remote Sensing*, 38(3), 1379–1386. <https://doi.org/10.1109/36.843032>
 Kouba, J. (2008). Implementation and testing of the gridded Vienna Mapping
 Function 1 (VMF1). *Journal of Geodesy*, 82(4), 193–205.
<https://doi.org/10.1007/s00190-007-0170-0>
 Lambin, J., Morrow, R., Fu, L.-L., Willis, J. K., Bonekamp, H., Lillibridge, J., et al.
 (2010). The OSTM/Jason-2 Mission. *Marine Geodesy*, 33(sup1), 4–25.
<https://doi.org/10.1080/01490419.2010.491030>
 Li, W., Yuan, Y., Ou, J., Li, H., & Li, Z. (2012). A new global zenith tropospheric
 delay model IGGtrop for GNSS applications. *Chinese Science Bulletin*, 57(17),
 2132–2139. <https://doi.org/10.1007/s11434-012-5010-9>
 Liu, Y., Liu, Y., Chen, G., & Wu, Z. (2019). Evaluation of HY-2A satellite-borne
 water vapor radiometer with shipborne GPS and GLONASS observations over
 the Indian Ocean. *GPS Solutions*, 23(3), 87.
<https://doi.org/10.1007/s10291-019-0876-5>
 Maiwald, F., Montes, O., Padmanabhan, S., Michaels, D., Kitiyakara, A., Jarnot, R.,
 et al. (2016). Reliable and stable radiometers for jason-3. *IEEE Journal of
 Selected Topics in Applied Earth Observations and Remote Sensing*, 9(6),
 2754–2762.
 Niell, A. E., Coster, A. J., Solheim, F. S., Mendes, V. B., Toor, P. C., Langley, R. B.,

- 613 & Upham, C. A. (2001). Comparison of Measurements of Atmospheric Wet
614 Delay by Radiosonde, Water Vapor Radiometer, GPS, and VLBI. *Journal of*
615 *Atmospheric and Oceanic Technology*, 18(6), 830–850.
616 [https://doi.org/10.1175/1520-0426\(2001\)018<0830:COMOAW>2.0.CO;2](https://doi.org/10.1175/1520-0426(2001)018<0830:COMOAW>2.0.CO;2)
- 617 Ruf, C. S., Keihm, S. J., Subramanya, B., & Janssen, M. A. (1994).
618 TOPEX/POSEIDON microwave radiometer performance and in-flight
619 calibration. *Journal of Geophysical Research: Oceans*, 99(C12), 24915–24926.
620 <https://doi.org/10.1029/94JC00717>
- 621 Saastamoinen, J. (1972). Atmospheric Correction for the Troposphere and
622 Stratosphere in Radio Ranging Satellites. *Geophys. Monogr. Ser.*, 15, 247–
623 251.
- 624 Sibthorpe, A., Brown, S., Desai, S. D., & Haines, B. J. (2011). Calibration and
625 Validation of the Jason-2/OSTM Advanced Microwave Radiometer Using
626 Terrestrial GPS Stations. *Marine Geodesy*, 34(3–4), 420–430.
627 <https://doi.org/10.1080/01490419.2011.584839>
- 628 Wang, J., & Liu, Z. (2019). Improving GNSS PPP accuracy through WVR PWV
629 augmentation. *Journal of Geodesy*.
630 <https://doi.org/10.1007/s00190-019-01278-2>
- 631 Wang, J., Wu, Z., Semmling, M., Zus, F., Gerland, S., Ramatschi, M., et al. (2019).
632 Retrieving Precipitable Water Vapor From Shipborne Multi-GNSS
633 Observations. *Geophysical Research Letters*, 46(9), 5000–5008.
634 <https://doi.org/10.1029/2019GL082136>
- 635 Wang, J., Dai, A., & Mears, C. (2016). Global Water Vapor Trend from 1988 to 2011
636 and Its Diurnal Asymmetry Based on GPS, Radiosonde, and Microwave
637 Satellite Measurements. *Journal of Climate*, 29(14), 5205–5222.
638 <https://doi.org/10.1175/JCLI-D-15-0485.1>
- 639 Zhang, L., Wu, L., & Gan, B. (2013). Modes and Mechanisms of Global Water Vapor
640 Variability over the Twentieth Century. *Journal of Climate*, 26(15), 5578–
641 5593. <https://doi.org/10.1175/JCLI-D-12-00585.1>